2014

Numerical and Experimental Analysis of Heat and Mass Transfer Processes on Water Trays in Household Refrigerators

Adriano Francisco Ronzoni
Federal University of Santa Catarina, Brazil, adriano@polo.ufsc.br

Cláudio Melo
Federal University of Santa Catarina, Brazil, melo@polo.ufsc.br

Carolin Ries
Europaische Studienakademie Kalte, Carolin.Ries@liebherr.com

Numerical and Experimental Analysis of the Heat and Mass Transfer Processes on Defrosted Water Trays of Household Refrigerators

Adriano F. RONZONI[1], Cláudio MELO[1]*, Carolin RIES[2]

[(1)]POLO - Research Laboratories for Emerging Technologies in Cooling and Thermophysics
Department of Mechanical Engineering, Federal University of Santa Catarina
88040-900, Florianópolis, SC, Brasil, +55 48 3234 5691

[(2)] ESaK - European Academy of Refrigeration and Air Conditioning
63477 Maintal, Germany, +49 7352 928 4599

* Corresponding author: melo@polo.ufsc.br

ABSTRACT

This paper describes an experimental and theoretical analysis of the heat and mass transfer processes that take place during defrosted water evaporation from compressor water trays. The influence of the operating conditions on the water evaporation rate was experimentally evaluated using a purpose-built testing facility. Two different tray designs were studied (top hat and membrane). In total, 16 experiments were carried out with the water evaporation rate varying from 4 g/h to 37 g/h. It was found that the compressor shell temperature was up to 11.6ºC lower and the average water evaporation rate was up to 109.5% higher in the membrane tray design. A dynamic simulation model was also developed and used to predict both the compressor shell temperature and the water evaporation rate. The model results were compared with the experimental data and over 80% of the model predictions for the average water evaporation rate lay within a 15% error band. It was also found that the water and compressor shell temperatures were predicted with maximum root mean square errors (RMSEs) of approximately 1.4ºC and 3.2ºC, respectively.

1. INTRODUCTION

Typical household refrigerators usually work according to the vapor compression principle and are comprised of four main components, namely: compressor, evaporator, capillary tube and condenser. The evaporator of most modern refrigerators is a forced-draft tube fin heat exchanger. The refrigerated compartments are kept at the desired temperatures as warm humid air from the fresh-food compartment and cold dry air from the freezer compartment are both cooled and dehumidified in the evaporator. During this process, frost accumulates on the cold evaporator surface due to desublimation of the water vapor contained in the air. This frost accumulation, which is a consequence of the cooling and dehumidifying process, is undesired, since the frost layer not only adds extra thermal resistance to the heat transfer process but it increases the evaporator pressure drop, both of which have a negative impact on the cooling capacity (Knabben *et al.,* 2011). Defrost heaters are thus regularly used in order to avoid excessive frost accumulation on the evaporator surface. To this end a timer is normally used to automatically activate the defrost cycle at a fixed time interval or according to the compressor run-time. During the defrosting process water drops from the evaporator surface and drains through a pipe into a water tray which is usually placed in the vicinity of the compressor. The evaporation of defrosted water into the ambient air takes place naturally as heat is transferred from the surroundings to the water contained in the tray. Typically, the hot compressor shell is the main heat source that drives the evaporation process. This system of defrosting and evaporation works well in places with low relative humidity, where the amount of defrosted water is lower and the evaporation rate is higher than those found in places with high relative humidity (Bansal and Xie, 2000). In areas with high relative humidity the frost accumulation will be higher and the defrosted water evaporation rate lower, and this may lead to water overflow after some defrost cycles. This is unacceptable from the viewpoint of both the refrigerator manufacturers and the costumers. Better and smarter ways of avoiding water overflow are therefore needed.

In spite of the fact that water overflow is an important issue for most refrigerator manufacturers, very few studies are available in the open literature (Bansal and Xie, 1998; Bansal and Xie, 1999; Xie and Bansal, 2000; Wongwises and Anansauwapak, 2005).

Bansal and Xie (1998) proposed an empirical correlation to predict the water evaporation rate from small exposed water surfaces, which is valid for both still air and air velocities of up to 5.36 m/s. A domestic freezer was used as the test section and the air temperature and velocity, the relative humidity and the water evaporation rate were determined. Three tests were performed with the air temperature and relative humidity close to 30ºC and 85%, respectively. Bansal and Xie (1999) put forward a dynamic simulation model to predict the defrosted water evaporation rate from water trays of domestic refrigerators. The model was used to analyze the effect of some design parameters (ambient temperature, relative humidity, air velocity, compressor heat, auxiliary condenser) on the water evaporation rate. Experiments were also carried out with a household refrigerator in order to provide the necessary data for the validation exercise. The compressor shell temperature was curve-fitted to the experimental results and used as input data during the simulations. Xie and Bansal (2000) developed an improved mathematical model by taking into account the thermal resistance between the compressor shell and the tray. Their model was successfully validated and it was able to predict the water evaporation rate to within ± 7.6% of the experimental data.

The experimental data available in the literature are rather limited and a dynamic simulation model to predict the defrosted water evaporation rate and its impact on the compressor shell temperature has yet to be developed. Both of these issues will be addressed in this article. To this end a purpose-built testing facility was designed and constructed to study the defrosted water evaporation process in a controllable manner. A dynamic simulation model was also developed to predict both the compressor shell temperature and the water evaporation rate from the condensing and evaporating pressure profiles. The model was validated against an experimental database comprised of 16 data points. Two different tray designs were studied, the top hat tray and the membrane tray. The experimental apparatus was placed in a climate-controlled room where the ambient temperature, relative humidity and air velocity were varied between the following values: $25ºC < T_{air} < 35ºC$, $45\% < \phi_{air} < 85\%$, $0.25 < V_{air} < 3.0$ m/s. The experiments were planned according to the factorial design technique (Box *et al.,* 2005), in order to rationalize the number of experimental data runs.

2. EXPERIMENTAL WORK

2.1 Experimental Facility

The experimental part of this study was carried out with a purpose-built testing facility essentially comprised of a HC-600a hot gas-cycle calorimeter, shown schematically in Figure 1. The test rig is driven by a 5.19 cm^3 variable-speed hermetic reciprocating compressor. The discharge and suction pressures are measured by strain gage absolute pressure transducers with maximum uncertainties of ±900 Pa and ±650 Pa, respectively. The discharge and suction temperatures are measured by T-type immersion thermocouples with a maximum uncertainty of ±0.2ºC. The refrigerant mass flow rate is measured by a Coriolis mass flow meter (MFM) with a maximum uncertainty of ± 0.06 kg/h. The discharge and suction pressures are controlled by two solenoid proportional valves (DPV and SPV), installed downstream and upstream of a medium pressure receiver (MPR), respectively. A water-cooled tube-in-tube counter-flow heat exchanger (HX) and an electric heater (SLH) are both used to control the compressor suction temperature. A thermostatic bath supplies cold water to the heat exchanger and also to a secondary loop used to refill the tray in a controlled manner.

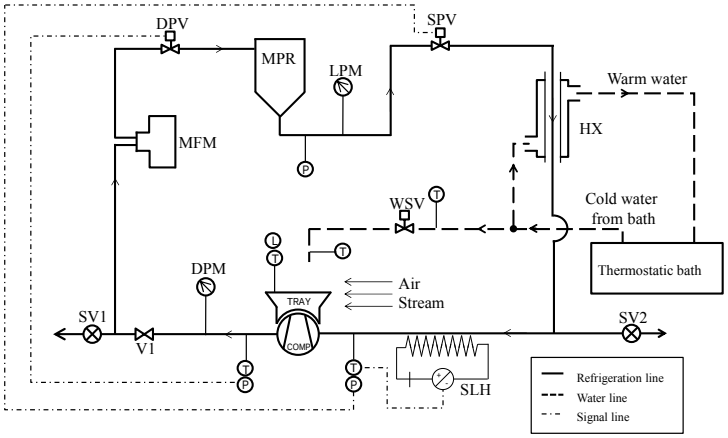

Figure 1: Schematic representation of the test set-up

2.2 Test Section

The test section (Figure 2) was comprised of a water tray installed at the top of the compressor. Five T-type thermocouples were installed at the top and two were installed in the middle of the compressor shell. The water temperature was measured by four T-type thermocouples. The air flow rate was supplied by a remotely controlled electronic centrifugal fan. The air velocity was measured beforehand by six anemometers and cross-correlated with the input voltage. This correlation was later used to set the desired air velocity. Air humidity and temperature probes with a maximum uncertainty of ±1.7% and ± 0.2ºC, respectively, were also installed in the test section. Finally, an ultrasonic sensor with an uncertainty of ± 0.2 mm was used to measure the water level during the evaporation process.

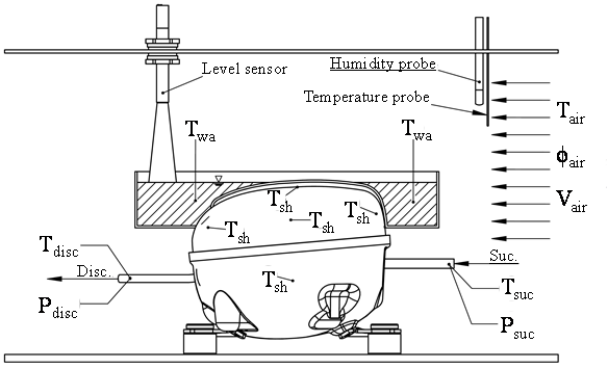

Figure 2: Schematic view of the test section

As previously mentioned only two tray designs were studied herein. A CAD (Computer Aided Design) model was used to define the tray geometry, as shown in Figure 3. Both trays were manufactured using a SLS (Selective Laser Sintering) technique and were made of polyamide-12 with 2 mm thick rigid frame walls. For the membrane tray, the rigid interface wall was replaced by a 0.2 mm-thick flexible polyvinyl chloride film.

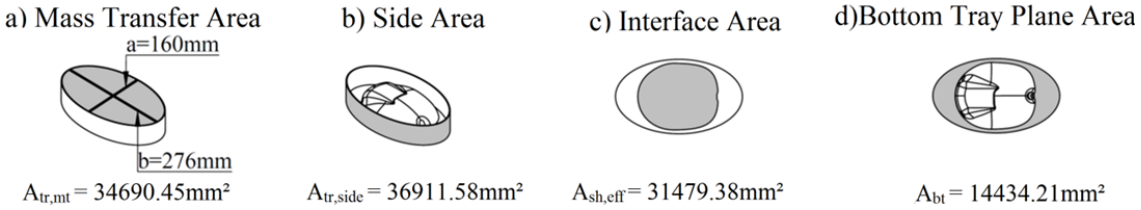

Figure 3: Tray geometry

2.3 Test Plan

The tests were carried out applying two different values for the air temperature (25ºC and 35ºC), relative humidity (45% and 85%) and air velocity (0.25 m/s and 3.0 m/s) and with the two tray designs, resulting in 16 experimental data points. Additionally, different values for the compressor on time t_{on} [h] and duty-cycle τ (the ratio between the compressor on time and the total cycle time, t_{total} [h]) were used for each air temperature while the compressor speed N_{comp} [Hz] was held constant.

The tests started with a mass of water ($M_{wa,o}$) of 800 g and lasted for 12 h. To reproduce a typical defrosting process, the thermostatic bath and the water solenoid valve were adjusted to supply a mass of water (M_{def}) of 100 g at 12ºC (T_{def}) for approximately 800 s, every 5 hours and 40 min (Δt_{def}). The experimental design and test conditions are summarized in Table 1, where T_{air} is the air temperature [ºC], ϕ_{air} the relative humidity [%] and V_{air} the air velocity [m/s].

Table 1: Experimental plan and test conditions

Test no.	Tray	T_{air} [ºC]	ϕ_{air} [%]	V_{air} [m/s]	t_{total} [h]	τ[-]	N_{comp} [Hz]
1	Top hat	25.0	45	3.00	1.0	0.50	50
2			85	3.00			
3			45	0.25			
4			85	0.25			
5	Membrane		45	3.00			
6			85	3.00			
7			45	0.25			
8			85	0.25			
9	Top hat	35.0	45	3.00	1.5	0.75	
10			85	3.00			
11			45	0.25			
12			85	0.25			
13	Membrane		45	3.00			
14			85	3.00			
15			45	0.25			
16			85	0.25			

3. SIMULATION MODEL

As previously mentioned, a semi-empirical dynamic simulation model was also developed to predict the compressor shell temperature and the water evaporation rate. The mathematical model was divided into two domains referred to as the water and compressor sub-models. The control volumes used for the modeling exercise are shown in Figure 4.

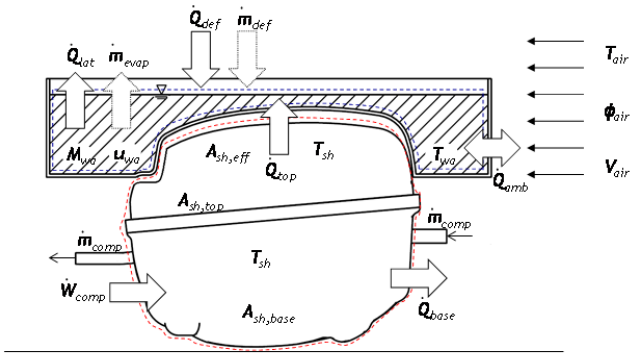

Figure 4: Water and compressor shell control volumes

3.1 Water Temperature Sub-model

In order to predict the water temperature and evaporation rate, a mathematical model was developed based on the earlier studies of Bansal and Xie (1999), Xie and Bansal (2000) and Wongwises and Anansauwapak (2005). The mass and energy conservation equations, when applied to the defrosted water control volume illustrated in Figure 4, can be expressed as:

$$\frac{d}{dt}\left(M_{wa}\right) = \dot{m}_{def} - \dot{m}_{evap} \tag{1}$$

$$\frac{d}{dt}\left(M_{wa}u_{wa}\right) = \dot{Q}_{def} - \dot{Q}_{lat} - \dot{Q}_{amb} + \dot{Q}_{top} \tag{2}$$

where M_{wa} is the mass of water contained in the tray [kg], u_{wa} is the defrosted water specific internal energy [J/kg], $\dot{m}_{def}$ is the defrosted water mass flow rate [kg/s] and $\dot{m}_{evap}$ is the water evaporation rate [kg/s].
The first term on the right-hand side of equation (2) represents the advective heat transfer due to the defrosted water mass flow rate, being expressed as:

$$\dot{Q}_{def} = \left(\frac{G_{def}}{t_{def}} \right) \cdot h_{def} \tag{3}$$

where h_{def} is the defrosted water specific enthalpy [J/kg], G_{def} is the amount of defrosted water [kg] and t_{def} is the defrosting period [s].

The second term on the right-hand side of equation (2) represents the evaporative latent heat loss, which can be expressed as:

$$\dot{Q}_{lat} = \frac{d}{dt}\left(M_{evap} \cdot h_{evap} \right) \tag{4}$$

where M_{evap} is the amount of water evaporated during a certain time interval [kg] and h_{evap} is the specific enthalpy of the saturated vapor at the water temperature [J/kg].

In accordance with Bansal and Xie (1999), the evaporated water mass flow rate can be expressed as:

$$\frac{d}{dt}\left(M_{evap} \right) = A_{tr,mt} \cdot c_1 \cdot \left[\left(c_2 + c_3 \cdot V_{air}^{c_4} \right) \cdot \left(p_{wa} - p_p \right) \right] \tag{5}$$

where $A_{tr,mt}$ is the water free surface area [m^2], V_{air} is the air velocity [m/s], p_{wa} is the water saturation pressure [Pa], p_p is the partial pressure of the water vapor in the surrounding air [Pa] and c_1=2.083x10^{-6}, c_2=0.002198, c_3=0.0398, c_4=0.5756.

The third term on the right-hand side of equation (2) represents the sensible heat exchange with the ambient air, which can be expressed as:

$$\dot{Q}_{amb} = \hbar_{air,free} \cdot A_{tr,mt} \cdot \left(T_{wa} - T_{air} \right) + U_{lat} \cdot A_{tr,side} \cdot \left(T_{wa} - T_{air} \right) + \varepsilon \cdot \sigma \cdot A_{tr,mt} \cdot \left(T_{wa}^4 - T_{air}^4 \right) \tag{6}$$

where T_{wa} is the tray average water temperature [K], T_{air} is the air temperature [K], ε is the water emissivity, σ = 5.67x10^{-8} [W/m^2·K^4] is the Stefan-Boltzmann constant, $A_{tr,side}$ is the side area of the tray [m^2], $\hbar_{air,free}$ is the convective heat transfer coefficient between the air stream and the water free surface (Churchill and Ozoe, 1973) and U_{lat} is the overall heat transfer coefficient [W/m^2·K] between the air stream and the water contained in the tray, expressed as:

$$\frac{1}{U_{lat}} = \left(\frac{1}{\hbar_{air}} + \frac{t_{wall}}{k_{wall}} + \frac{1}{h_{wa}} \right) \tag{7}$$

where t_{wall} is the thickness of the rigid tray frame [m], k_{wall} is the thermal conductivity of the tray material [W/m·K], $\hbar_{air}$ is the convective heat transfer coefficient between the air stream and the water contained in the tray (Jakob, 1949) and $\hbar_{wa}$ is the natural convective heat transfer coefficient (McAdams, 1954).

Finally, the last term on the right-hand side of equation (2) represents the heat transfer between the hot compressor shell and the water in the tray, which can be expressed as:

$$\dot{Q}_{top} = U_{sh} \cdot A_{sh,eff} \cdot \left(T_{sh} - T_{wa} \right) \tag{8}$$

$$\frac{1}{U_{sh}} = \left(R''_{t,c} + \frac{t_{\text{int}}}{k_{\text{int}}} + \frac{1}{h_{wa}} \right) \tag{9}$$

where U_{sh} is the overall heat transfer coefficient between the compressor shell and the water in the tray [W/m^2·K], $A_{sh,eff}$ is the effective heat transfer area (interface area [m^2], in Figure 3), t_{int} is the interface thickness [m], k_{int} is the thermal conductivity of the interface material [W/m·K] and $R''_{t,c}$ is the thermal contact resistance [m^2·K/W].

The overall heat transfer coefficient between the compressor shell and the water in the tray (U_{sh}) was determined from the experimental data (tests 2, 3, 14 and 15 in Table 1), according to Equation (10), and used to calculate the thermal contact resistance according to Equation (9).

$$U_{sh} = \frac{\hbar_{air,free} \cdot A_{tr,mt} \cdot (T_{wa} - T_{air}) + U_{lat} \cdot A_{tr,side} \cdot (T_{wa} - T_{air}) + \varepsilon \cdot \sigma \cdot A_{tr,mt} \cdot (T_{wa}^4 - T_{air}^4) + \dot{m}_{evap} \cdot h_{evap}}{A_{sh,eff} \cdot (T_{sh} - T_{wa})} \tag{10}$$

Finally, the rate of the temperature change of the water contained in the control volume illustrated in Figure 4 can be expressed as:

$$\frac{dT_{wa}}{dt} = \frac{\dot{Q}_{top} + \dot{Q}_{def} - \dot{Q}_{amb} - u_{wa} \cdot \dot{m}_{def} + (u_{wa} - h_{evap}) \cdot \dot{m}_{evap}}{M_{wa} \cdot c_{v,wa} + M_{evap} \cdot Z} \tag{11}$$

and

$$Z = c_{p,wa} + \left(\frac{\partial h_{fg}}{\partial p_{ev}} \right) \cdot \left(\frac{dp_{ev}}{dT_{ev}} \right) + \left(\frac{\partial h_{fg}}{\partial T_{ev}} \right) \tag{12}$$

where $c_{p,wa}$ and $c_{v,wa}$ are, respectively, the water specific heat at constant pressure and volume [J/kg·K], h_{fg} is the latent heat of evaporation [J/kg], p_{ev} is the saturation pressure and T_{ev} is the saturation temperature.

3.2 Compressor Temperature Sub-model

Applying the first law of thermodynamics to the compressor control volume indicated in Figure 4 results in:

$$\frac{dT_{sh}}{dt} = \frac{\dot{m}_{comp} (h_{suc} - h_{disc}) + \dot{W}_{comp} - \dot{Q}_{top} - \dot{Q}_{base}}{C_{comp}} \tag{13}$$

where C_{comp} is the compressor heat capacity [J/K], T_{sh} is the average compressor shell temperature [K] and h_{suc} and h_{disc} are the specific enthalpy of the refrigerant at the suction and discharge pipes [J/kg], respectively.

The refrigerant mass flow rate, $\dot{m}_{comp}$ [kg/s], and the compressor power, $\dot{W}_{comp}$ [W], can both be expressed in terms of the volumetric and global efficiencies as follows:

$$\dot{m}_{comp} = \eta_{vol} \left\{ \left[\left(\frac{\pi \cdot D_{cil}^2}{4} \right) \cdot L_{cil} \right] \frac{N_{comp}}{v_{suc}} \right\} \tag{14}$$

where η_{vol} is the volumetric efficiency, D_{cil} and L_{cil} are the piston diameter and stroke [m], N_{comp} is the compressor speed [Hz] and v_{suc} is the specific volume of the refrigerant [m^3/kg].

$$\dot{W}_{comp} = \frac{\dot{m}_{comp}}{\eta_g} \cdot \left\{ p_{suc} \cdot v_{suc} \cdot \left(\frac{n}{n-1} \right) \left[\left(\frac{p_{disc}}{p_{suc}} \right)^{\left(\frac{n-1}{n} \right)} - 1 \right] \right\} \quad (15)$$

where n is the polytropic exponent and η_g is the global efficiency. It should be noted that the compressor volumetric (η_{vol}) and global (η_g) efficiencies were adjusted to the manufacturer's data for the calorimeter as proposed by Jähnig (2000).

The terms $\dot{Q}_{top}$ and $\dot{Q}_{base}$ in Equation (13) represent the compressor heat loss to the water in the tray (equation 8) and the heat exchanges with the surrounding air, the latter being expressed as:

$$\dot{Q}_{base} = U_{sh,base} \cdot A_{sh,base} \left(T_{sh} - T_{air} \right) \quad (16)$$

where $A_{sh,base}$ is the fraction of the compressor shell that is not in contact with the tray and $U_{sh,base}$ is the overall heat transfer coefficient between the exposed shell and the surrounding air [W/m^2·K], derived from the experimental data and expressed as:

$$U_{sh,base} = \frac{\dot{m}_{comp} \left(h_{suc} - h_{disc} \right) + \dot{W}_{comp} - \dot{Q}_{top}}{A_{sh,base} \cdot \left(T_{sh} - T_{air} \right)} \quad (17)$$

3.3 Solution Scheme

The previous set of equations has to be solved in order to calculate the time evolution of the water and compressor shell temperatures as well as of the water evaporation rate. To this end, the following input data are required: initial mass of water, initial water temperature, initial compressor shell temperature, air temperature, relative humidity, air velocity, compressor speed and the suction and discharge pressure profiles. The compressor and the tray geometry must also be supplied as input data in order to completely define the problem. The suction and discharge pressure profiles were curve-fitted to the experimental data for each air temperature. The difference between the discharge and shell temperatures, $\Delta T_{disc\text{-}sh}$ [K], was assumed to have a time-dependent linear relationship (*i.e.*, $\Delta T_{disc\text{-}sh} = b + a \cdot t_{comp}$) where a and b are fitted constants and t_{comp} is the compressor running time. At each time step, equations (11) and (13) are integrated over time using a forward explicit Euler scheme with a fixed time step.

4. RESULTS AND DISCUSSION

All 16 data points were used in the validation exercise. However, only 4 tests were used to derive the empirical parameters U_{sh} and $U_{sh,base}$. The model predictions for the average water evaporation rate are compared with the experimental data in Figure 5a and a good agreement can be observed, with over 80% of the data points falling within a 15% error band. Figure 5b shows the root mean square error (RMSE) for the water and compressor shell temperatures. It is worth noting that the model predictions are in reasonable agreement with the experimental data, with maximum RMSE values of around 1.4ºC and 3.2ºC for the water and compressor shell temperatures, respectively.

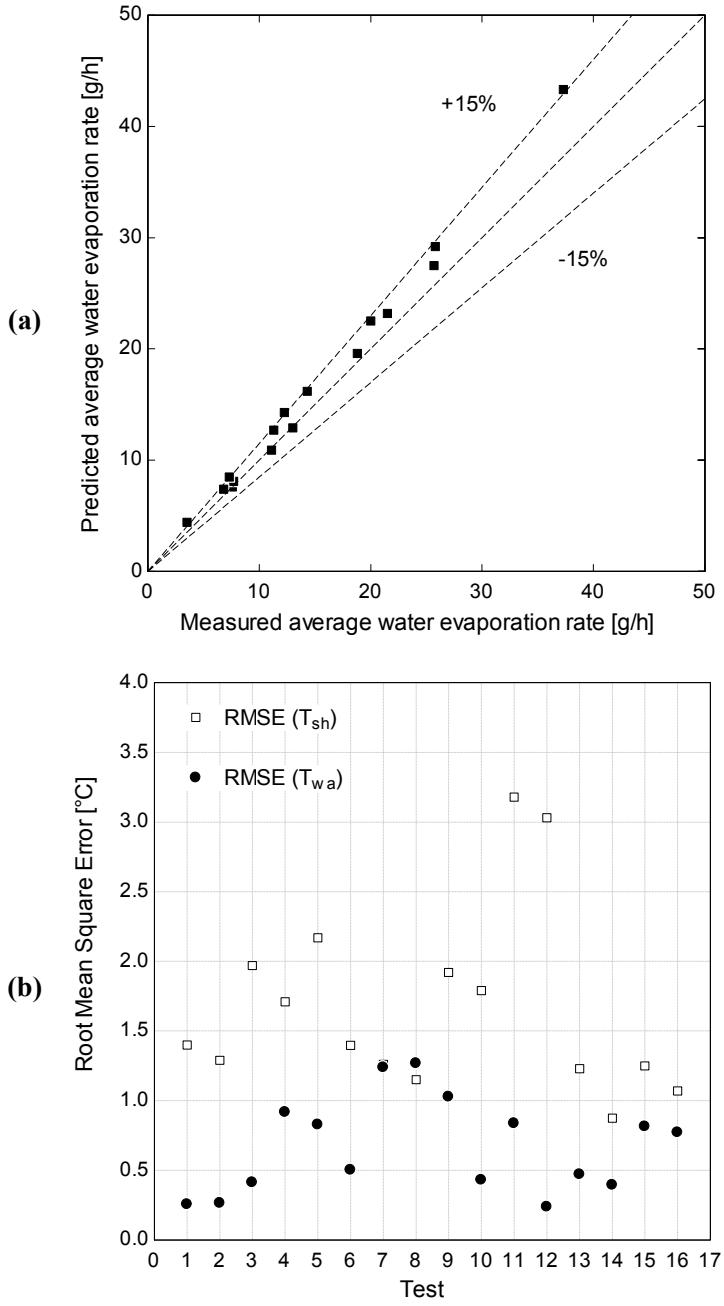

Figure 5: Model Predictions: (a) average water evaporation rate and (b) RMSEs of shell and water temperatures

Figure 6 shows the time evolution of the compressor shell temperature (Figure 6a), water temperature (Figure 6b) and mass of water (Figure 6c) for both tray designs (tests 4 and 8 of Table 1). As shown in Figure 6a, the model closely predicts the compressor shell temperature profile during the on and off compressor cycles. It can also be observed that the compressor shell temperature is 8.0ºC lower, the water temperature is 4.0ºC higher and the water evaporation rate is 109.5% higher in the membrane tray compared with the top hat design. This is due to the lower thermal resistance between the compressor shell and the tray. Overall, a maximum compressor shell temperature drop of 11.6°C, a maximum water temperature increase of 5.7ºC and a maximum water evaporation increase of 109.5% were found when comparing the two tray designs under the same operating test conditions.

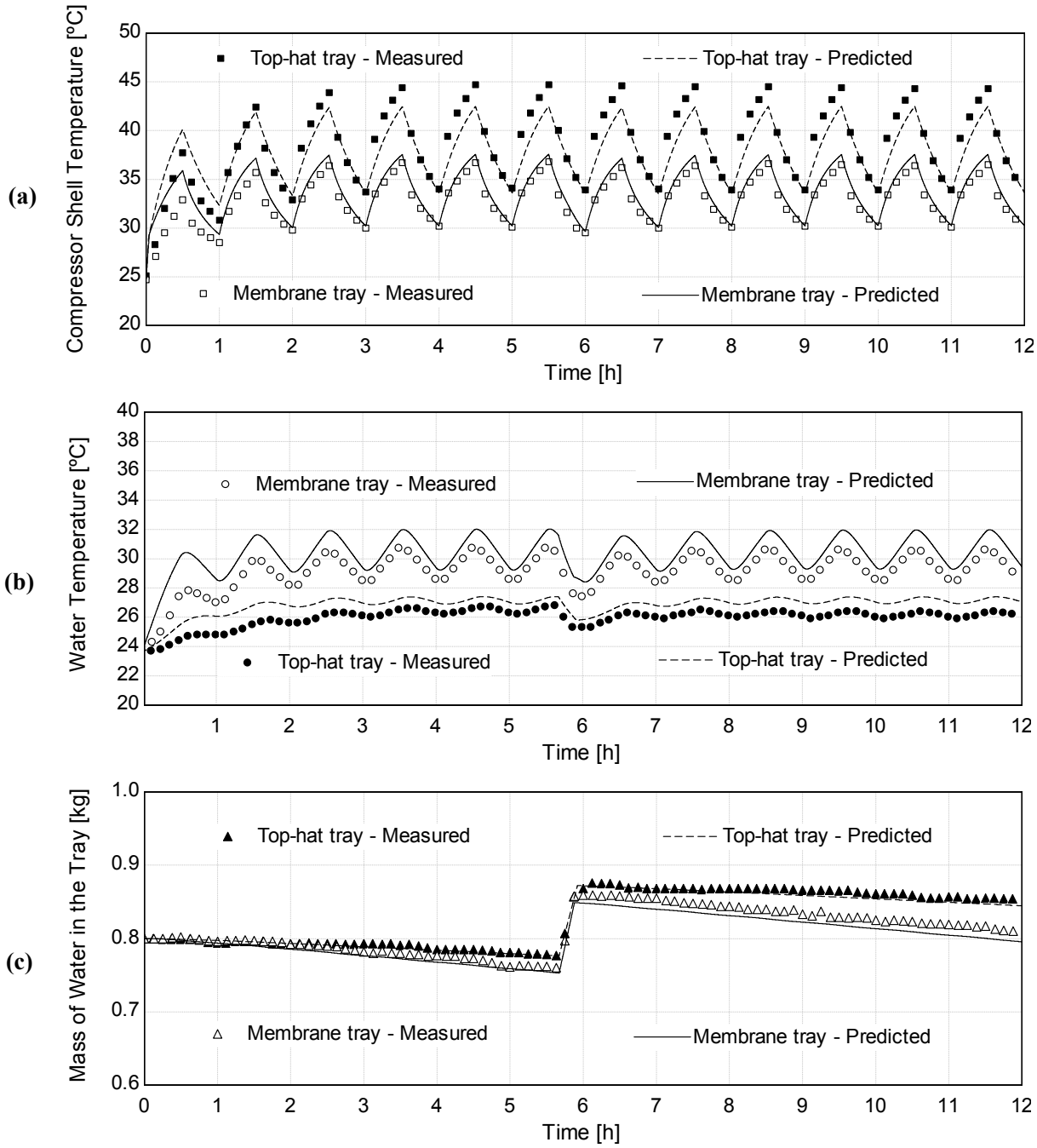

Figure 6: Time evolution of the predicted and measured results:
(a) compressor shell temperature, (b) water temperature and (c) mass of water in the tray

5. CONCLUSIONS

A purpose-built test facility was designed, constructed and used to study the heat and mass transfer processes associated with defrosted water trays of household refrigerators. The experiments were carried out with two tray designs, the top hat and the membrane tray. In total, 16 experimental data points were obtained under different operating conditions. A semi-empirical dynamic simulation model based on the governing mass and energy conservation equations was developed to predict the compressor shell temperature and the water evaporation rate. Four steady-state tests were used to define the compressor/tray thermal resistance and the compressor shell overall heat transfer coefficient. The water and the compressor shell temperatures were integrated over time through the Euler forward scheme, while the water evaporation rate was calculated from the empirical correlation proposed by Bansal and Xie (1998). The model predictions were compared with the experimental data and it was observed that over 80% of the data points for the average water evaporation rate lay within a 15% error band. The water and the compressor shell temperatures were also well predicted by the model, with maximum RMSE values of around 1.4ºC and 3.2ºC, respectively. Furthermore, it was shown that the water evaporation rate increases by up to 109.5% and the compressor shell temperature decreases by up to 11.6ºC when the top hat tray is replaced by the membrane tray design. The current model can thus be used to predict the water evaporation rate for different compressor/tray designs under a wide range of operating conditions, thereby reducing the need for the time consuming experimental overflow tests commonly used by most refrigerator manufacturers.

REFERENCES

Bansal, P. K., Xie, G., 1998, A Unified Empirical Correlation for Evaporation of Water at Low Air Velocities, *Int. Commun. Heat Mass.,* vol. 25, no. 2: p. 183-190.

Bansal, P. K., Xie, G., 1999, A Simulation Model for Evaporation of Defrosted Water in Household Refrigerators, *Int. J. Refrig.,* vol. 22, no.4: p. 319-333.

Box, G. E. P., Hunter, J. S., Hunter, W. G., 2005, *Statistics for Experimenters – Design, Innovation and Discovery*, 2nd ed, John Wiley and Sons, New York, 639 p.

Churchill, S. W., Ozoe, H., 1973, Correlations for Laminar Forced Convection in Flow Over an Isothermal Flat Plate and in Developing and Fully Developed Flow in an Isothermal Tube, *J. Heat Trans.- T. ASME*, vol. 95, no.3: p. 416–419.

Jähnig, D. I., Reindl, D.T., Klein, S.A., 2000, A Semi-Empirical Method for Representing Domestic Refrigerator / Freezer Compressor Calorimeter Test Data, *ASHRAE Trans*., vol. 106, pt. 2.

Jakob, M., 1949, *Heat Transfer*, vol. 1, John Wiley and Sons, New York, 758 p.

Knabben, F. T., Hermes, C. J. L., Melo, C., 2011, In-situ Study of Frosting and Defrosting Processes in Tube-Fin Evaporators of Household Refrigerating Appliances, *Int. J. Refrig*., vol. 34, no. 8: p. 2031-2041.

McAdams, W. H., 1954, *Heat Transmission*, 3rd ed., McGraw-Hill, New York, 532 p.

Wongwises, S., Anansauwapak, B., 2005, Prediction of Evaporation of Defrosted Water in Refrigerator Water Trays, *Int. Commun. Heat Mass*, vol. 32, no 4: p. 403-415

Xie, G.; Bansal, P. K., 2000, Analysis of Defrosted Water Evaporation from Three Water Trays in Refrigerators. *Appl. Therm. Eng.*, vol. 20, no. 7, p. 651-669

ACKNOWLEDGEMENTS

This study was carried out at the POLO facilities under National Grant No. 573581/2008-8 (National Institute of Science and Technology in Refrigeration and Thermophysics) funded by the Brazilian Government Agency CNPq. The authors are grateful to Messrs. Guilherme Zanotelli dos Santos and Yuri Lima Modolon for their valuable support in the experiments. Financial support from Embraco is also duly acknowledged.